DINCON'09
8TH BRAZILIAN CONFERENCE ON DYNAMICS, CONTROL AND APPLICATIONS
MAY 18-22, 2009

ORTOGONAL DISCRETE WAVELET DECOMPOSITION: PART 1. USING ACE SATELLITE DATA.

Ojeda, A G. [1, 6], *Correa, M. S.* [2], *Klausner, V.* ,[1, 3], *Domingues, M.O* [4] , *Mendes, O. Jr.* [5] , *Papa, A. R. R.* [3, 7]

[1] National Institute for Space Research – INPE/CEA/GES, São José dos Campos-SP, Brazil, aojeda78@gmail.com
[2] National Institute for Space Research – INPE/CTE/CAP, São José dos Campos-SP, Brazil, rizesimoes@uol.com.br
[3] National Observatory – ON/MCT, Rio de Janeiro, Rio de Janeiro, Brazil. virginia@on.br, papa@on.br
[4] National Institute for Space Research – INPE/CTE/LAC, São José dos Campos-SP, Brazil, margarete@lac.inpe.br
[5] National Institute for Space Research – INPE/CEA/DGE, São José dos Campos-SP, Brazil, odim@dge.inpe.br
[6] Institute of Geophysics and Astronomy – IGA/CITMA, Havana City, Cuba, arian@iga.cu
[7]Universidade do Estado do Rio de Janeiro – IF, Rio de Janeiro-RJ, Brazil

Abstract: We analyze geomagnetic disturbance using ACE satellite and Dst data (April 2001). The Daubechies orthogonal wavelet transform has been chosen because of its ability to analyze non-stationary signals and time-frequency localization. The wavelet coefficients thresholds allow the singularity detection in the solar wind component associate with a future geomagnetic storm.

Keywords: Wavelet analysis, Multi-resolution analysis; Sun–Earth coupling.

1. INTRODUCTION

The solar plasma expands out from the Sun driven by thermo-electrodynamical processes. The solar magnetic field propagates "frozen" in the solar wind in a spiral-like configuration due to the Sun's rotation. When this solar plasma in expansion arrives at the Earth intrinsic magnetic field, a substantial transfer of energy into the terrestrial magnetosphere may take place. Then, the normally existing magnetospheric and ionospheric quiet currents are widened and intensified. These current systems are related to magnetic disturbance phenomena that are called, geomagnetic storms and geomagnetic substorms respectively (e.g. [1]). The characteristic signature of a magnetic storm is a depression in the horizontal component of the Earth's magnetic field H at middle to low latitude ground station. This depression is shown by the Dst index. The key parameters that control the solar wind magnetospheric coupling are the strength and the direction of the interplanetary magnetic field (IMF). For example intense magnetic storm (Dst<-100 nT) are caused by an IMF southward component stronger than 10 nT at least for 3 h (e.g. [2]). Solar wind speed and density also play a role in the formation of the ring current, though their exact role is still controversial (e.g. [2-5]).

In high latitude a large horizontal currents flow in the D and E regions of the auroral ionosphere, called Auroral Electrojet. During disturbed periods, these currents are intensified and their limits can extend beyond the auroral region. This expansion is mostly caused by enhanced particle precipitation and enhanced ionospheric electric fields. These currents are related to auroral geomagnetic disturbances, called geomagnetic substorms (e.g. [6]). To characterize the global electrojet activity in the auroral zone is widely used the Auroral Electrojet (AE) index, originally introduced by [7]. The energy budget and substorms size are largely controlled by processes driven directly by the solar wind (e.g. [8]).

An important solar event is the coronal mass ejection (CME) because it can cause geomagnetic storms. They are observed near 1AU and are called interplanetary coronal mass ejections (ICMEs). The term magnetic cloud (MC) is used to characterize an ICME having a specific configuration of IMF and plasma density (e.g. [9-11]). The MCs have values of plasma beta significantly lower than 1. Near 1 AU MCs have enormous radial sizes (0.28 AU), with an average duration of 27 h, an average peak magnetic field strength of 18 nT and the average solar wind speed 420 km/s (e.g. [10], [12-13]). In [13] first suggested that MCs are force-free magnetic field configurations ($\nabla \times B = \alpha(r) B$). The constant α solution for a cylindrical symmetric force-free equation was given by [14] and is a constant related to the size of a flux rope.

In this paper we work with time series of solar wind variables where its future behavior cannot be predicted exactly, as would be the case for a deterministic function of time. Nondeterministic (random) processes may be categorized as being either stationary or nonstationary. Stationary random processes may be further categorized as being either ergodic or nonergodic. Nonstationary random processes may be further categorized in terms of specific types of nonstationary properties. These are generally time-varying functions that can be determined only by performing instantaneous averages over the ensemble of sample functions forming the process. In practice, it is often not feasible to obtain a sufficient number of sample records to permit the accurate measurement of properties by ensemble averaging. That fact has tended to impede the development of practical techniques for measuring and analyzing nonstationary random data. In many cases, the nonstationary random data produced by actual physical phenomena can be classified into special categories of nonstationarity that simplify the measurement and analysis problem.

Time series models are used for a variety of purposes. Some of the most common of these are prediction, estimation of transfer functions, filtering and control, simulation and optimization and generating new physics theories. Time series analysis is now widely used in many

studies of space geophysics (e.g. [15-17]). One important aspect is spectral analysis, because it is concerned with the splitting up of the time into different frequency components.

The analyses of ACE satellite data corresponds to an analysis of a random or non-deterministic time series. The characteristic of this kind of series is that the future behavior cannot be predicted. In this case, our series is also non-stationary in such a way that its properties change with time. Then, the Fourier and Wavelet techniques have been chosen (e.g. [18]) to identify hidden frequencies in solar wind data. Those frequencies can be useful to study the physics of the system. The two techniques cannot predict the behavior of the system but help to detect singularities in signal and transient structures (e.g. [19]) related to geomagnetic disturbances.

Wavelet and Fourier detect frequency but give different information. The wavelet transform can be used in the analysis of non-stationary signals to obtain information on the frequency or scale variations of those signals and to detect their structures localization in time and/or in space (e. g. [18]). The last properties are impossible to be recognized with Fourier transform, only the presence of involved frequencies is detected. The wavelet transform is a transform that preserves the energy, and then in analogy with the terminology adopted in Fourier analysis, the squared modulus of the wavelet coefficients is called scalogram.

2. PURPOSE

The purpose of this work is to analysis the relationship between solar wind parameters and geomagnetic storms in term of time series features. The implemented methodology is the wavelet technique (Daubechies orthogonal wavelet transform) as an alternative way to identify quiescent from non-quiescent periods in solar wind data that triggered geomagnetic disturbances.

Domingues et al. [18] and Mendes et al. [19] detected disturbances in X or H components of magnetograms using wavelet coefficients amplitude. In other words, they examined "the effect" of the solar wind –magnetosphere interaction. In this work we are examining features related to "cause" of the geomagnetic storms. They are two moments of unique physical system. For this reason, with this exploration study we hope to obtain good results with wavelet technique.

3. DATA AND METHODS

The Daubechies orthogonal wavelet transform is the main method applied in this work. Previously it was necessary to prepare the data for processing. Next we will explain that:

3.1. ACE satellites data

The geomagnetic activity during April 2001 an arbitrary selected period will be study in this paper using ACE satellite data and Dst index available at the NOAA web site http://spidr.ngdc.noaa.gov/spidr/index.jsp 2008 ([20]). All time series represent physical parameters with 1 min resolution.

The ACE satellites data at the NOAA web site http://spidr.ngdc.noaa.gov/spidr/index.jsp 2008 ([20]) are present in Geocentric Solar Ecliptic (GSE) coordinates system. We used a routine written in Wolfram Mathematica 6.0 ([21]) to transform GSE to Geocentric Solar Magnetic (GSM) system according to the method proposed by Hapgood [22-23] and enhanced by Franz and Harper [24]. The GSE system is defined such that the x axis is directed towards the Sun while the y axis lies in the ecliptic plane in the direction opposite to the Earth's velocity around the Sun; the z axis completes the right-hand system (z = x × y) which places it essentially along the ecliptic North pole. The origin is located at the centre of the Earth. The GSE system is not inertial, making a full rotation about the z axis in one year.

The GSM system differs from GSE by a rotation about the x axis such that the terrestrial magnetic dipole lies in the +zx plane. That is, GSM z axis is the projection of the magnetic dipole onto the GSE yz plane. In addition to the annual rotation, this coordinate system exhibits a diurnal wobble. Since the magnetic dipole is usually taken from a geomagnetic model, there can be disagreements between investigators according to which one they use.

For two vectors (X_{se}, Y_{se}, Z_{se}), (X_{sm}, Y_{sm}, Z_{sm}) in GSE and GSM coordinates respectively, the matrix of coordinates transform is T3 = <-ω, X> (e. g. [22]), then:

$$\begin{cases} X_{sm} = X_{se} \\ Y_{sm} = Y_{se}\cos\omega - Z_{se}\sin\omega \\ Z_{sm} = Y_{se}\sin\omega + Z_{se}\cos\omega \end{cases} \quad (1)$$

Where ψ lies between +90 and -90° and is the angle between the GSE z axis and projection of the magnetic dipole axis on the GSE yz plane (i.e. the GSM z axis) measured positive for rotation towards the GSE y axis. It can be calculated by:

$$\omega = Arc\tan(y_e / z_e) \quad (2)$$

The procedure to calculus of y_e and z_e was developed in [22], the final expression is:

$$\begin{cases} y_e = \cos\theta\cos\lambda_0\cos\xi\cos\varphi\sin\lambda \\ \quad\quad -\sin\theta\sin\lambda_0\cos\varphi\cos\lambda \\ z_e = \cos\xi\sin\varphi \end{cases} \quad (3)$$

$\lambda_0 \rightarrow$ Is the Sun ecliptic longitude, that depend the Sun's mean anomaly (M), mean longitude (Λ) and the time in Julian centuries (T_0).

$\xi \rightarrow$ The obliquity of the ecliptic.

$\theta \rightarrow$ The matrix <θ, Z> corresponds to a rotation in the plane of the Earth's geographic equator from the First Point of Aries to the Greenwich meridian. The rotation angle θ is the Greenwich mean sidereal time.

$\lambda \rightarrow$ Geocentric longitude of the dipole North geomagnetic pole.

$\phi \rightarrow$ Geocentric latitude of the dipole North geomagnetic pole.

Hapgood [22] used the first order coefficients (g_1^0, g_1^1, h_1^1) of the International Geomagnetic Reference Field (IGRF) for the year 1985 (e.g. [25]), and derived approximations to calculate λ and ϕ. We used IGRF for 2005 ([26]) to this

calculus and derived the following approximation (see [24] for IGRF 2000):

$$\begin{cases} \lambda = 288^o.421 - 0^o.0434183\, y_0 \\ \varphi = 79^o.5241 + 0^o.0354527\, y_0 \end{cases} \quad (4)$$

Where y_0 are Julian years from J2000. The equations were obtained by a linear adjustment through the list of values to IGRF coefficients 1975-2005 (seven points).

3.2. Discrete Wavelet Transform (DWT).

The wavelets transforms were better and broadly formalized thanks to mathematicians, physicist, and engineers efforts (e.g. [27]). In space geophysics applications, the main characteristic of the wavelet technique is the introduction of time-frequency decomposition (e.g. [18] and [19]). In the 1990s several important ideas and applications concerning wavelet were developed (e.g. [28-33]).

The wavelet analysis could show that the larger amplitude of the wavelet coefficients are associated with abrupt signal locally. In other work, the transition region and the presence of the involved frequencies are detected.

The multiresolution analysis is a mathematical tool using to build wavelet function ([28], [31], [34]).

A multiresolution analysis (AMR) a pair $\{V^j, \phi^j\}$, the vector spaces embebed forms by two subspaces $V^j \subset V^{j+1}$, with $V^j = span\{\phi_k^j(t)\}$ and ϕ_k^j an scale function, more details in Mallat [34]:

$$\phi(t) = 2\sum_{k\in Z} h(k)\phi(2t-k) \quad \text{(Scale relation)} \quad (5)$$

Where h(k) is called scale filter coefficients ψ_k^j. The family of function forms a Riesz base of V^j:

$$\phi_k^j(t) = 2^{j/2}\phi(2^j t - k), \quad j,k \in Z \quad (6)$$

They are called scale function, where in frequency domain is:

$$\hat{\phi}(\xi) = H(\xi/2)\hat{\phi}(\xi/2) \quad (7)$$

$$H(\xi) = \sum_{k\in Z} h(k)e^{-ik\xi} \quad \text{(Low pass filter associate to } \phi)$$

The following relation holds:

$$V^{j+1} = V^j \oplus W^j. \quad (8)$$

The spans W^j have the difference of information between V^j and V^{j+1}. The ψ function form the Riez basic of W^j. They are called wavelet function:

$\psi_k^j(t) = 2^{j/2}\psi(2^j t - k)$ *and* $\psi(x) = 2\sum g(h)\phi(2x-h)$ where $g(h) = (-1)^{k+1}h(-k+1)$. The wavelet and scale functions satisfy the orthogonality condition,

$$\begin{aligned} &<\phi_k^j, \psi_l^j> = 0, \\ &<\psi_k^j, \psi_l^m> = \delta_{j,m}\delta_{m,l} \end{aligned} \quad (9)$$

The Amr tool is useful to study the function in $L^2(R)$. The difference of information between V^j and V^{j+1} is given by

Where the projections in V^j and W^j are:

$$\Pi^j f(t) = \sum_k \left\langle f, \Phi_k^j \right\rangle \Phi_k^j(t), \quad (10)$$

$$Q^j f(t) = \sum_k \left\langle f, \psi_k^j \right\rangle \psi_k^j(t), \quad (11)$$

respectively.

We obtain in multi-level $j_0 < j$ the coefficients expression:

$$c_k^j = \left\langle f, \phi_k^j \right\rangle, \quad d_k^j = \left\langle f, \psi_k^j \right\rangle, \quad (12)$$

We can obtain with a change of base $\{\phi_k^{j+1}\} \leftrightarrow \{\phi_k^{j_0}\} \cup \{\psi_k^{j_0}\} \ldots \cup \{\psi_k^j\}$ in equation (13):

$$\sum_k c_k^{j+1}\phi_k^{j+1}(t) = \sum_k c_k^{j_0}\phi_k^{j_0}(t) + \sum_{m=j_0}^{j}\sum_k d_k^m \psi_k^m(t) \quad (13)$$

In the DWT the equation (12) is manipulated jointly to the scale relations:

$$\begin{aligned} c_k^j &= \sqrt{2}\sum_m h(m-2k)c_m^{j+1} \\ d_k^j &= \sqrt{2}\sum_m g\ (m-2k)c_m^{j+1} \end{aligned} \quad (14)$$

In this work we use the Daubechie wavelet function of order 2. In this case the coefficients h = [0.482963, 0.836516, 0.224144, -0.129410] and g = [-0.129410, -0.224144, 0.836516, -0.482963].

Its methodology was used in this work. Its implementation to process the data was based on the following ([19]): "To calculate the discrete wavelet transform in the temporal series, to analyze the wavelet coefficients of the decomposition levels and to choose the wavelet coefficient thresholds that allow the singularity detection in solar wind events associated with the correspond geomagnetic disturbance identified by Dst Index. In the characterization of a solar wind disturbance, all the squared wavelet coefficients greater than the chosen threshold are considered. In this analysis, the threshold has been defined as the minimum value of the square coefficients that exceeds the local background fluctuations. Then, a new time series was constructed using the inverse discrete wavelet transform that sets to zero the other wavelet coefficients not associated with the solar wind disturbance. The reconstructed and the original series were then compared to determine the amount of energy lost, considering the L^2 norm."

4. RESULTS

In April 2001 happened seven sudden storm commencing (SSC) identified in the Dst Index (Fig. 1). These events occurred during the solar maximum of the 23th solar cycle. Some ICME that caused geomagnetic disturbances were studied in [35] and [5].

They identified MCs by a different methodology that can be found in their papers. Table 1 shows one MC identified in [35] and three MCs identified in [5] respectively. We had preference by [5] because they used ACE satellites data while [35] used WIND data. The minimum Dst index is important to characterize the geo-effectiveness of MCs. According to [36] and [37] the geomagnetic response of a certain MC depends greatly on its flux-rope structure (Table

1, column 5). Table 2 shows geomagnetic disturbance detected in the Dst Index not associated with MCs. The minimum Dst index was presented.

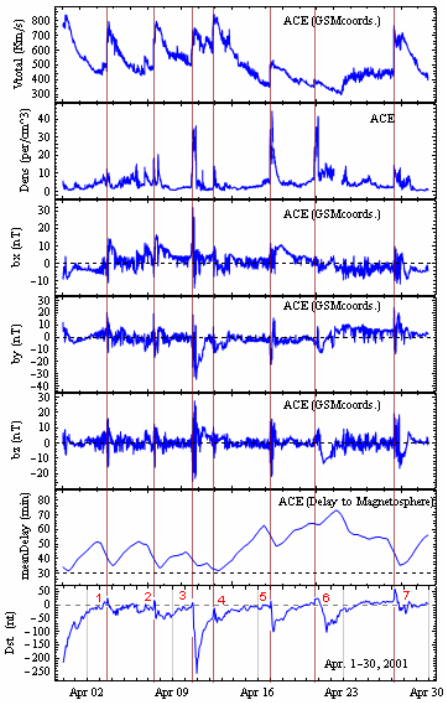

Fig. 1. Dataset to characterize the global geomagnetic disturbance in April 2001. This time window show seven geomagnetic storm with different degree of disturbance (Dst<-100, degree of disturbance extreme). The storms were enumerated from 1 to 7 for a better interpretation of the results. One extreme storm happened with a minimum Dst= -256 nT at 23:00 UT on April 11. ACE satellites data has time resolution of 1 min and it is presented in GSM coordinates.

Fig.1 shows the behavior of the solar wind parameters of April 2001. In each panel, from top to bottom, total velocity, plasma density, IMF components (bx, by, bz in GSM coordinate), mean delay to magnetosphere and also the Dst index, for different solar wind events. We represented lines (from bottom to top) to identify the sudden storms commencing (SSC) in the Dst Index. The solar wind events were enumerates from left to right (1 to 7) to relate with the descriptions shows in Tables 1 and 2 (column 1) respectively. As can be noted from this figure, the signatures of the seven geomagnetic disturbances identity by Dst index are not identical. The variations of the solar wind components are not identical to seven events. If wavelet techniques identify such different behaviors then it will bring a lot of help to study the solar wind-magnetosphere interaction. The time windows selected show different level of disturbances in the geomagnetic field (Degree of disturbance of Dst Index). This is perfect to validate the wavelet methology. We can compare the amplitude of wavelet coefficients among all events. Then, we should find some physical explication for the Sun–Earth coupling.

Fig.2 shows the behavior of the square wavelet coefficients for the solar wind parameters of April 2001 at levels j = 1, 2, 3, denoted by d1, d2, d3. In each panel, from top to bottom, the Dst index, the solar wind parameter (IMF components, total velocity or density) and the first three levels of the wavelet coefficients of the discrete wavelet transform (see equation 14) are shown (similar methodology was applied in [19] to study X or H component of the geomagnetic field for five stations). The letters (a)-(e) stand for the solar wind parameters (to ACE satellites) bx, by, bz, velocity and density, respectively. After ~30 minutes these solar events (See Fig. 1, delay to magnetosphere) cause different levels of disturbances in the geomagnetic field.

The variations in the ring current are associated with magnetic field fluctuations on the grounds that are depicted by the Dst index. On the other hand, these fluctuations are related to energy variations in the ring current, controlled by processes driven directly by the solar wind. In [19] were detected such disturbances in X or H component of magnetograms with wavelet coefficients. In other words, they found "the effect" of the solar wind –magnetosphere interaction. In this work we are searching "the cause" of geomagnetic storms.

The wavelet coefficients in Fig. 2 identified solar wind events of different properties and degrees of disturbance. The wavelet coefficients have maximum amplitude those identity geoeffectiveness solar wind events. The coefficients (d1, d2, d3) have differences for single events and others respectively. In the maximum of solar activity the solar wind is very disturbed. Generally, models that predict geomagnetic activity work well at minimum solar activity. Then, the capacity of wavelet method to work correctly in high solar activity is an important advantage for its future use as a sophisticated space weather tool.

We developed a methodology (effectiveness coefficients (EC)) to interpret the results shown in Fig. 2. The effectiveness coefficients method (see table 3) corresponds to the following: All numbers have two digits (nm) where the first digit, represent the quantity of wavelet coefficients that identified the solar wind event. The second digit, inform how many wavelet coefficients have amplitude bigger that twice the background. If $0 \leq n \leq 3$ then $0 \leq m \leq n$. Finally, $00 \leq nm \leq 33$. The possible values of nm are: 30, 31, 32, 33, 20, 21, 22, 10, 11, 00.

This method was applied visually but can be computational implemented to identify singularities in signal and transient structures that cause geomagnetic disturbance. Now, it can help to interpret the results because we can compare their effectiveness among parameters (Table. 3, end row) and events (Table. 3, end column). The possible maximum value to end row is 33*7 = 231 and to end column is 33*5= 165. The wavelet coefficients distinguish better quiescent from non-quiescent periods in IMF components than velocity and density. For example, larger amplitude in the wavelet coefficients to IMF components is related with the strong geomagnetic storm of day 11.

5. DISCUSSION

In [19] it was found that, "when a geomagnetic storm is under development (disturbed periods) the wavelet coefficients are significantly large". The previous idea is applied to solar wind parameters with 30 min delay time approximately to the beginning storm the propose had simply to characterize the quiescent and non-quiescent periods, the discrete wavelet transform (Daubechies) is a sophisticated space weather tool still in development and we are working to help to characterize the geomagnetic disturbance with this methodology.

Table 1. MCs Identified in ACE and WIND data to April 2001 ([35] and [5]). The columns from the left to the right give: Solar wind events enumerated from left to right and shows in Fig. 1, shock date (day and hour (UT)), MC start date (day and hour (UT)), MC end date (day and hour (UT)), inferred flux-rope type (e.g. [5]), the minimum value of the Dst index, it date of the previous one (day and hour (UT), if the sheath caused the storm, it is indicated by "sh"), satellite data to identified the MCs (Wind (W), ACE (A)).

No.	Shock	MC, Star	MC, Stop	type	Dstmin	Dstmin date	ST
1	04, 14:54	04, 20:54	05, 08:24	----	-039	05, 07:00	W
3	11, 15:18	12, 10:00	13, 06:00	WNE	sh(-256)	11, 23:00	A
6	21, 15:06	21, 23:00	22, 24:00	WSE	-103	22, 15:00	A
7	28, 04:31	29, 00:00	29, 13:00	SEN	-33	29, 03:00	A

Table 2. Geomagnetic disturbance detected in the Dst Index not associated with MCs. The columns from the left to the right give: Solar wind events enumerate from left to right and shows in Fig. 1, Dst value in the sudden storm commencing (SSC), date of the SSC (day and hour (UT)), the minimum value of the Dst index after the SSC, it date of the previous one (day and hour (UT)).

No.	SSC Dst	SSC date	Dstmin	Dstmin date
2	017	08, 11:00	-054	09, 07:00
4	-012	13, 10:00	-066	13, 15:00
5	015	18, 01:00	-101	18, 06:00

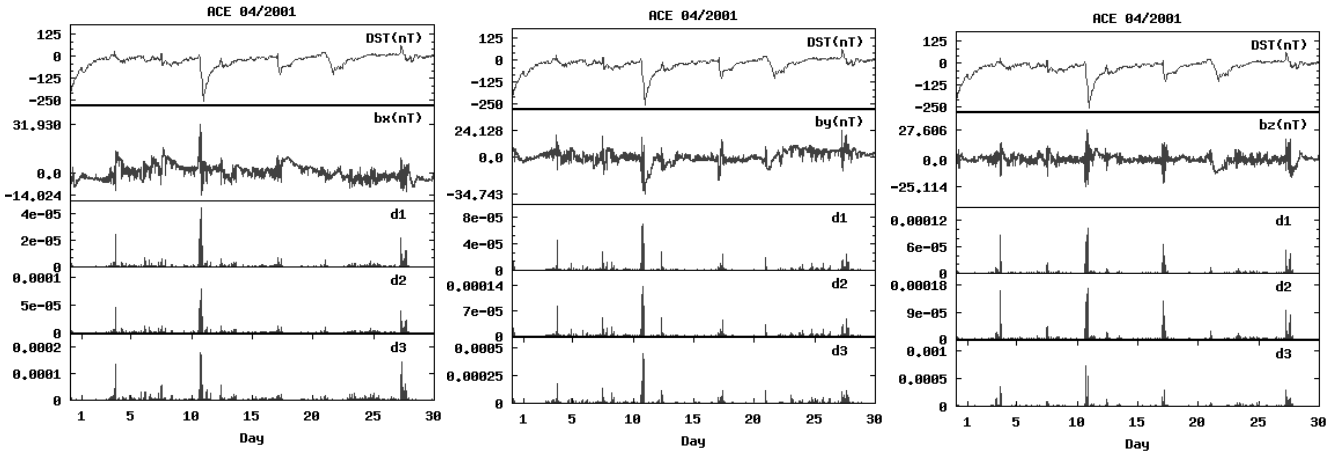

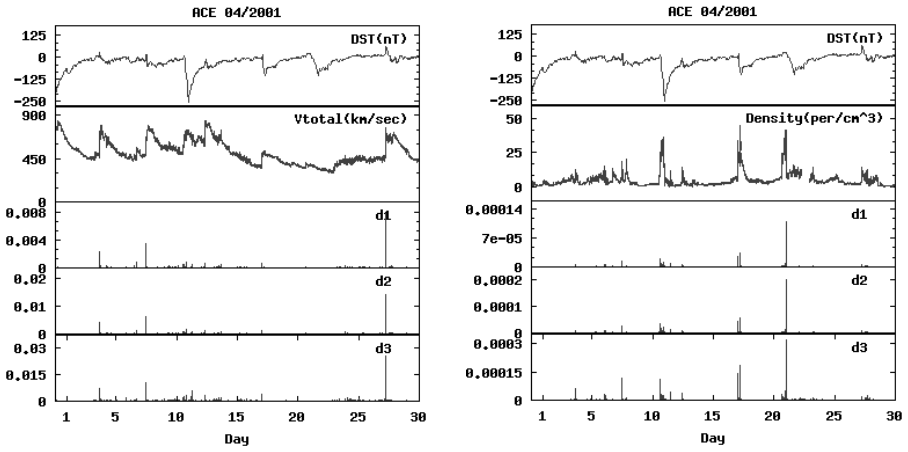

Fig. 2. ACE satellites dataset and Dst index for April 2001. The letters (a)-(e) stand for bx, by, bz, total velocity and plasma density. Each panel shows from top to bottom, the Dst index, the solar wind parameter (IMF components, density or velocity) and the first three levels of the wavelet coefficients (showing with reduction factor of 104) of the discrete wavelet transform.

The highest amplitudes of the wavelet coefficients indicate singularity and in all cases singularity patterns were identified in association with solar wind events.

In the WSE-type MC the magnetic field vector rotates from the west (W) at the leading edge to the east (E) at the trailing edge, being south (S). Also, the z- component has the same sign during de MC and has the axis highly inclined to the ecliptic (Unipolar MCs). The MC WNE-type ([37]) that caused one extreme storm happened with a minimum Dst = -256 nT (shock) at 23:00 UT on April 11, ACE. The wavelet coefficients has high amplitude in this date, it is bigger than other events to IMF components. Plasma density and velocity don't fulfill these previous remarks. Then, the cause of the extreme storm is the reconnection, in other words; the event is more magnetic than kinetic.

The number 7 (see Fig. 1) geomagnetic storm was caused by a MC SNE-type (See table 1). The event was very magnetic and wavelet detected that (table 3, IMF components with number codec 33). But this event had plasma density smaller than number 3. The wavelet coefficient had number codec 30; it detected the low density of the event. It event caused medium degree of disturbance of Dst index according to NOAA classification (Dst = - 33 nT). This could be a consequence of the low values of plasma density associated with this particular event in the solar wind. In general, the statistic is poor to make some conclusion about flux rope type in the MCs related with the wavelet coefficients. We did not find relation among wavelet coefficients and flux rope type in MCs. The MC with WSE flux rope type was the worse identity (by wavelet) among all events.

Table 2. Effectiveness coefficients to validate the wavelet technique for detects singularities in signal and transient structures that cause geomagnetic disturbance. The end column is the somatorium of the rows (to four parameters) for each event (seven). The end row is the somatorium of the column elements (to seven events) for each parameter (four). The explication of the effectiveness coefficients is shown in the text.

Event.	bx	by	bz	Dens	Vtotal	Sum. rows
1	33	33	33	31	33	163
2	31	33	33	33	33	163
3	33	33	33	33	31	163
4	31	33	33	31	32	160
5	32	33	33	33	33	164
6	22	33	32	33	20	140
7	33	33	33	30	33	162
Sum. Col.	215	231	230	224	215	

The wavelet coefficients presented more frequently higher amplitude to IMF component than plasma density and velocity. They don't always show this characteristic, depends if the interplanetary disturbance is magnetic (reconnection), kinetic (viscous-type interactions) or a mixture of both cases.

The ACE satellite was localized in the Lagrangian Point L1, then it detect de solar event 30 – 45 min before arriving to the Earth Magnetosphere. If the DWT was applied online then it could help to forecast a future geomagnetic disturbance. The results presented in this study are not conclusive. We need to improve the statistics.

A study about the surface effect recorded in magnetograms data of the seven solar wind event is presented by Klausner et al. [38] for the same period. That study was realized with the same methodology (DTW) applied in this work. Thus, the both works are useful to implement the DWT tool to predict global geomagnetic disturbance.

6. FINAL REMARKS

1. The wavelet technique is useful to "zoom in" the localized behavior of the interplanetary solar plasma data; i. e., the identification of transients related to the geomagnetic storms.

2. The discrete wavelet transform (Daubechies) is an alternative way to predict the global geomagnetic disturbance and it could be used as a sophisticated space weather tool still in development.

3. The higher amplitude of the wavelet coefficients (IMF components, density or velocity) occurred during shock of solar wind events.

4. The wavelet coefficient thresholds allow the detection of singularities in the solar wind component associated with a future geomagnetic storm.

5. The effectiveness coefficient methodology suggested in this paper represents another way of looking the results and can be used in other applications.

ACKNOWLEDGMENTS

This work was supported by CNPq (309017/2007-6, 486165/2006-0 and 308680/2007-3), FAPESP (2007/07723-7) and CAPES. The authors wish to thank SPIDR-Boulder and WDC-Kyoto for the datasets used in this work.

REFERENCES

[1] Y. Kamide, N. Yokoyama, W. Gonzalez, B. T. Tsurutani, I. A. Daglis, A. Brekke and S. Masuda, "Two-step development of geomagnetic storms," J. Geophys. Res., Vol. 103, pp. 6917–6921, 1998.

[2] W. T. Gonzalez and B. T. Tsurutani, "Criteria of interplanetary parameters causing intense magnetic storms (Dst<-100 nT)," Planet. Space Sci., Vol. 35, pp. 1101–1109, 1987.

[3] F. R. Fenrich and J. G. Luhmann, "Geomagnetic response to magnetic clouds of different polarity," Geophys. Res. Lett. Vol. 25, pp. 2999–3003, 1998.

[4] C. B. Wang, J. K. Chao and C.-H. Lin, "Influence of the solar wind dynamic pressure on the decay and injection of the ring current," J. Geophys. Res., Vol. 108, No. A9 pp. 1341 doi:10.1029/2003JA009851, 2003.

[5] K. E. J. Huttunen, R. Schwenn, V. Bothmer and H. E. J. Koskinen, "Properties and geoeffectiveness of magnetic clouds in the rising, maximum and early declining phases of solar cycle 23," Annales Geophysicae Vol. 23, pp. 1–17, 2005.

[6] O. Mendes, A. Mendes da Costa and F. C. P. Bertoni, "Effects of the number of stations and time resolution on Dst derivation," J. of Atm. and Solar-Terrestrial Physics, Vol. 68, No. 18, pp. 2127-2137,2006.

[7] T. N. Davis and M. Sugiura, "Auroral Electrojet Activity Index AE and Its Universal Time Variations", Journal of Geophysical Research, Vol. 71, p.785, 1966.

[8] E. Tanskanen, T. I. Pulkkinen, H. E. J. Koskinen, and J. A. Slavin, Substorm energy budget during low and high solar activity: 1997 and 1999 compared, J. Geophys. Res., Vol. 107, No. A6, pp.1086, doi:10.1029/2001JA900153. 2002.

[9] L. Burlaga, E. Sittler, F. Mariani, and R. Schwenn, "Magnetic loop behind an interplanetary shock: Voyager, Helios and IMP 8 observations," J. Geophys. Res., Vol. 86, pp. 6673–6684, 1981.

[10] L. W. Klein, and L. F. Burlaga, "Interplanetary magnetic clouds at 1AU," J. Geophys. Res., Vol. 87, pp. 87 613–87 624, 1982.

[11] J. T. Gosling, "Coronal mass ejections and magnetic flux ropes in interplanetary space, in Physics of magnetic flux ropes," Geophys. Monorg. Ser., edited by Russel, C. T., Priest, E. R., and Lee, L. C., AGU, Washington D.C, Vol. 58, pp. 3518–3528, 1990.

[12] R. P. Lepping and D. Berdichevsky, "Interplanetary magnetic clouds, Sources, properties, modelling, and geomagnetic relationship," Recent Res. Devel. Geophys., Vol. 3, pp. 77–96, 2000.

[13] H. Goldstein, "On the field configuration in magnetic clouds, in Solar Wind," Five edited by Neugebauer, M., Geophys. NASA Conf. Publ, Vol. 22, pp. 731–733, 1983.

[14] S. Lundquist, "Magnetohydrostatic fields," Ark. Fys., Vol. 2, pp. 316–365, 1950.

[15] A. Calzadilla and B. Lazo, "Nonlinear Time Series Analysis of the Dst Geomagnetic Index," Sheeffield Space Plasma Meeting: Multipoint Measurements Versus Theory. ESA Publications Division, SP 492. 2001.

[16] A. G. Ojeda, A. Calzadilla, B. Lazo, K. Alazo and S. Savio, "Analysis of Behavior of Solar Wind Parameters Under Different IMF Conditions Using Two Nonlinear Dynamics Techniques," Journal of Atmospheric and Solar Terrestrial Physics, Vol. 67, pp. 1859-1864, 2005.

[17] A. R. R. Papa, L. M. Barreto and N. A. B. Seixas, "Statistical study of magnetic disturbances at the Earth´s surface," Journal of Atmospheric and Solar Terrestrial Physics, Vol. 68, pp. 930-936, 2006.

[18] M. O. Domingues, O. Mendes and A. Mendes da Costa; "Wavelet techniques in atmospheric sciences," Advances in Space Research Vol. 35, No. 5, pp 831–842, 2005.

[19] O. Mendes, M. O. Domingues and A. Mendes da Costa, "Wavelet analysis applied to magnetograms," Journal of Atmospheric and Solar-Terrestrial Physics, COLAGE special issue, in press, Vol. 67, pp. 1827–1836, 2005.

[20] SPIDR, http://spidr.ngdc.noaa.gov/spidr/index.jsp 2008.

[21] Wolfram Mathematica 6.0 (Version for window XP), 2008.

[22] M. Hapgood, "Space physics coordinate transformations: A user guide," Planet. Space Sci. Vol. 40, No. 5, pp. 711–717, 1992.

[23] M. Hapgood, "Corrigendum, space physics coordinate transformations," A user guide. Planet. Space Sci. Vol. 45, No.8, pp. 1047, 1997.

[24] M. Fränz and D. Harper, "Heliospheric Coordinate Systems," Planetary & Space Science, Vol. 50, pp. 217ff., 2002.

[25] A. C. Fraser-Smith, "Centered and Eccentric Geomagnetic Dipoles and Their Poles," 1600-1985, Reviews of Geophysics, Vol. 25, No. 1, pp 1-16, 1987.

[26] WDC-Kyoto, Available from: http://swdcwww.kugi.kyoto-u.ac.jp/index.html , 2008.

[27] J. Morlet, "Sampling theory and wave propagation," in: C.H. Chen, (Ed.), Acoustic Signal/Image Processing and Recognition, in NATO ASI. Springer-Verlag, New York, No. 1, pp. 233–261, 1983.

[28] I. Daubechies, "Ten lectures on wavelets," in: CBMS-NSF Regional Conference Series in Applied Mathematics, SIAM, Philadelphia, PA, Vol. 61, 1992.

[29] C. K. Chui, "An Introduction to Wavelets," Academic Press, San Diego, CA, Vol. 1, 1992.

[30] C. K. Chui, "Wavelets: A Tutorial in Theory and Applications," Academic Press, San Diego, CA, Vol. 2, 1992.

[31] B. Jawerth and W. Sweldens, "An overview of wavelet based multiresolution analysis," SIAM Review Vol. 36, No. 3, pp. 377–412, 1994.

[32] C. K. Chui, L. Montefusco and L. Puccio, "Wavelets Theory, Algorithms and Applications," Academic Press, San Diego, CA, Vol. 5, 1994.

[33] G. Strang and T. Nguyen, "Wavelet and Filters Bank," Welsley-Cambridge, Cambridge, 1996. Available from: http://saigon.ece.wisc.edu/waveweb/tutorials/book.html, 1996.

[34] S. Mallat, "Multiresolution approximations and wavelets orthonormal bases," Transactions of American Mathematical Society," Vol.315, pp. 334–351, 1991.

[35] C.-C. Wu, R. P. Lepping and N. Gopalswamy, "Variations of magnetic clouds and CMEs with solar activity cycle," in Proc. ISCS 2003 Symposium, "Solar variability as an input to the Earth's Enviroment", Slovakia, ESA, Vol. 1, pp. 429–432, 2003.

[36] G. Zhang and L. F. Burlaga, "Magnetic clouds, geomagnetic disturbances, and cosmic ray decreases," J. Geophys. Res., Vol. 93, pp. 2511–2518, 1988.

[37] V. Bothmer, "Sources of magnetic helicity over the solar cycle," Proc. ISCS 2003 Symposium, Tatranská Lomnica, Slovakia, 23-28 June 2003(ESA AP-535), September 2003.

[38] V. Klausner, M. S. Correa, A. G. Ojeda, M. O.